

Article

Study of Ionanofluids Behavior in PVT Solar Collectors: Determination of Thermal Fields and Characteristic Length by Means of HEATT[®] Platform

Mariano Alarcón ^{1,*}, Juan-Pedro Luna-Abad ², Manuel Seco-Nicolás ¹, Imane Moulefera ³
and Gloria Villora ³

- ¹ Electromagnetism and Electronics Department, International Campus of Excellence in the European Context (CEIR) Campus Mare Nostrum, University of Murcia, 30100 Murcia, Spain
- ² Thermal and Fluid Engineering Department, International Campus of Excellence in the European Context (CEIR) Campus Mare Nostrum, Technical University of Cartagena, 30202 Cartagena, Spain; jp.lunaabad@upct.es
- ³ Chemical Engineering Department, International Campus of Excellence in the European Context (CEIR) Campus Mare Nostrum, University of Murcia, 30100 Murcia, Spain; imane.moulefera@um.es (I.M.); gvillora@um.es (G.V.)
- * Correspondence: mariano@um.es; Tel.: +34-630521837

Abstract: Solar electric and solar thermal energies are often considered as part of the solution to the current energy emergency. The pipes of flat plate solar devices are normally heated by their upper surfaces giving rise to an asymmetric temperature field in the bulk of the fluid, which influences the heat transfer process. In the present work, a study of the characteristic length of tubes, or most efficient distance at which heat transfer occurs, in flat photovoltaic-thermal (PVT) hybrid solar devices has been carried out using three heat transfer fluids: water, [Emim]Ac ionic liquid and ionanofluid of graphene nanoparticles suspended in the former ionic liquid. The main objective of the study was to know whether the heat transfer occurs in optimal conditions. Experimental measurements have been made on a commercial PVT device, and numerical simulations have been performed using the HEATT[®] platform to determine the characteristic length of the process. The tests conducted showed a clear improvement in the temperature jump of the fluid inside the collector when INF is used compared to water and ionic liquid and even a higher overall energy efficiency. Electricity generation is not greatly affected by the fluid used, although it is slightly higher when water is used. Slower fluid velocities are recommended if high fluid outlet temperatures are the goal of the application, but this penalizes the overall thermal energy production. The characteristic process length is not typically achieved in parallel tube PVT collectors with ordinary flow rates, which would require a speed, and consequently, a flow rate, about 10 times lower, which penalizes the performance (up to four times), although it increases the fluid outlet temperature by 234%, which can be very interesting in certain applications. Ionanofluids may in the medium term become an alternative to water in flat plates or vacuum solar collectors for applications with temperatures close to or above 100 °C, when their costs will hopefully fall. The results and methodology developed in this work are applicable to solar thermal collectors other than PVT collectors.

Keywords: solar energy; photovoltaic-thermal collectors (PVT); characteristic length; ionanofluids; HEATT[®]



Citation: Alarcón, M.; Luna-Abad, J.-P.; Seco-Nicolás, M.; Moulefera, I.; Villora, G. Study of Ionanofluids Behavior in PVT Solar Collectors: Determination of Thermal Fields and Characteristic Length by Means of HEATT[®] Platform. *Energies* **2024**, *17*, 5703. <https://doi.org/10.3390/en17225703>

Academic Editor: Alan Brent

Received: 1 October 2024

Revised: 6 November 2024

Accepted: 8 November 2024

Published: 14 November 2024



Copyright: © 2024 by the authors. Licensee MDPI, Basel, Switzerland. This article is an open access article distributed under the terms and conditions of the Creative Commons Attribution (CC BY) license (<https://creativecommons.org/licenses/by/4.0/>).

1. Introduction

A consensus is emerging that renewable energies, and in particular energy from the sun, will play a central role in the context of the energy transition to a more sustainable model. This is evidenced by the growing body of literature on the subject, including references [1–4]. Solar energy is arguably the most pervasive, plentiful and cost-free energy

resource accessible to humanity [5–8]. Despite the fact that solar energy, encompassing both thermal and photovoltaic technologies, can be regarded as mature fields, it is evident that there is still considerable scope for enhancement in efficiency, particularly as new applications and demands emerge. Consequently, it is imperative to persist in research and integration of novel technologies to facilitate more effective utilisation of the solar resource [9].

As is well known, there are different ways of using solar energy. Low-temperature solar thermal energy obtained through flat plate collectors (FPSC) for the production of domestic hot water and other low-temperature applications was the most developed during the second half of the 20th century [10]. In the last 10 years, however, it is photovoltaic solar energy that has seen spectacular development, becoming one of the main sources of electricity generation in many countries [11].

One type of solar collector that is receiving increasing attention is the so-called hybrid photovoltaic-thermal (PVT or PV/T) collector [12], whose main attraction is that they simultaneously provide thermal and electrical energy, both of which are needed in multiple applications, both in the residential and service sectors and in industry [13]. It can be called a two-in-one panel. PVT collectors are receiving increasing interest, sometimes as a replacement for PV panels in several installations [14], as shown by the fact that this market is growing rapidly, with a growth rate of around 13% in 2021 [12]; hybrid collectors from different manufacturers and models can be found on the market [15].

In their most classic configuration, these panels are composed of a first layer of photovoltaic cells, under which there is a solar thermal collector very similar to the conventional FPSC, capable of collecting a good part of the solar radiation that the photovoltaic cells are not able to take advantage of [12,15]. The photovoltaic cells, capable of converting around 20% of the solar radiation into electrical energy, benefit from the cooling effect that the heat transfer fluid of the thermal part exerts on them, thus reducing their efficiency loss at high external temperatures, while the thermal part is adversely affected because it receives less solar radiation than it would if it did not have to pass through the layer of photovoltaic cells. However, this reduction in thermal efficiency is not very important because the temperatures reached in the absorber plate of the PVT collector, and consequently the heat losses, are lower than in the case of FPSC collectors. Consequently, the combined thermal-electrical efficiency of the PVT panel per unit area exceeds that of a photovoltaic or thermal panel, reaching up to 80% in certain applications [15]. Compared to photovoltaic collectors, the additional thermal output of hybrid systems makes them more cost-effective than stand-alone photovoltaic and thermal units with the same total aperture area [12].

There are currently many publications on PVT collectors, most of which use water as the heat transfer fluid [14,16,17]. Recently, several researchers have optimized the electrical and thermal production of hybrid collectors by modeling their operating conditions [18,19], including through artificial intelligence and machine learning [20].

Another line of research is that which explores new heat transfer fluids that improve the performance of PVT collectors, both in their function of cooling the photovoltaic cells and in their thermal production, in both cases to improve the efficiency of the whole, which is largely derived from the thermophysical properties of the fluid. As in FPSC, in PVT collectors, in addition to water, other fluids such as glycol solutions, brines or, more recently, nanofluids are used [21–23].

Nanofluids are a suspension of nanoscale particles (typically on the order of 10–50 nm) in a base fluid. The addition of suitable nanoparticles to a base fluid, such as water, can significantly improve its thermophysical properties [24]. For solar thermal or thermal-photovoltaic applications, usually the most significant property on which the performance of the collectors depends is the thermal conductivity of the heat transfer fluid [10]. In solar energy, nanoparticles of metals, metal oxides, graphene or other materials with high thermal conductivity have been used, which significantly increase, depending on their concentration and particle size, the thermal conductivity of the heat transfer fluid, so their effect is always beneficial [25,26].

Emmanuel et al. concluded that nanofluids of different types show better performance in PVT modules compared to other collector components due to their enhanced thermal conductivity that improves heat transfer as well as the cooling process of PV panels [15]. Said et al. found that the use of nanofluids typically improves the efficiency of the hybrid collector by more than 5% [27]. Abdelrazik et al. analytically evaluated the optical, stability and energy performance of water-based MXene nanofluids in a hybrid PVT collector, proving the suitability of this type of nanofluid for improving collector performance [28]. Aslfattahi et al. evaluated the performance enhancement of a concentrated photovoltaic thermal collector using MXene nanofluids employing silicone oil as their base fluid for applications up to 150 °C [29].

Water is a heat transfer fluid with thermal properties that are hard to overcome, although it has certain limitations such as a high vapor pressure, a relatively low boiling point and high melting point, corrosion, etc. FPSCs normally operate below 100 °C but can reach this temperature or higher in severe weather conditions or failures, with steam production, which can lead to plant shutdown and overheating [10]. Therefore, it is very interesting to use low vapor pressure fluids as the working fluid for medium-high temperature applications.

Ionic liquids (ILs) are organic salts that have a melting point below 100 °C, can remain in the liquid phase up to approximately 400 °C, and in many cases, their freezing points are below 0 °C. In addition, they have a very low vapor pressure, high thermal and chemical stability, and very important in practical applications, no corrosion problems. On the other hand, their thermal conductivity and specific heat are significantly lower than those of water, their viscosity much higher, and their price currently very high. On the other hand, ILs are also capable of suspending nanoparticles that improve their heat transfer properties so that they can approach those of water or other fluids, without losing their thermochemical advantages [30]. These properties make ILs, alone or as a base fluid for nanofluids, interesting candidates for use in solar energy in medium and even high temperature applications.

Nieto de Castro et al. [31] introduced the term ionanofluids (INFs) for a new generation of nanofluids where the ILs play the role of a base fluid. ILs have proven their suitability for producing very stable suspensions with many nanoparticles of different natures, which can significantly improve the thermophysical properties of the base fluid. Compared to ILs, INFs offer better thermal properties, specific heat and thermal conductivity, among other things, at low cost. Nanofluids can be made more stable by using ionic liquids, whose anions and cations provide an electrostatic layer around the nanoparticles that prevents them from accumulating [32]. Józwiak et al. [33] reported substantial increases in thermal conductivity of up to 70% with high aspect ratio carbon nanotubes (CNTs). In the case of graphene nanoplatelets (GNPs), remarkable increases in thermal conductivity of about 30% were observed [34]. Hasečić et al. numerically modeled and analyzed the heat transfer performances of ionic liquids [C4mpyrr][NTf2] and ionanofluids with Al₂O₃ nanoparticles under a laminar flow regime [35].

The use of ionanofluids in solar energy has not been widely cited to date. Das et al. numerically evaluated the behavior of a binary ionanofluid-based ionic liquid (IL) + water binary solution with two-dimensional MXene (Ti₃C₂) nanoadditives at different concentrations in a PV/T hybrid solar system, finding that the optimum concentration was 0.20 wt % [36]. Shaik et al. [32] modeled an artificial neural network and optimized the thermophysical behavior of MXene ionanofluids for solar photovoltaic-thermal hybrid systems by analyzing the nanoparticle concentration and temperature. Moulefera et al. have recently published the synthesis and characterization of different ionanofluids (INFs) based on 1-ethyl-3-methylimidazolium acetate ([Emim]Ac) ionic liquids (ILs) or [Emim]Ac/water mixtures as the base fluids and graphene oxide (GO) as nanoparticles, as well as their performance evaluation in an experimental flat plate solar thermal collector (FPSC) [9]. These works are an example of the interest in the use of INFs in solar energy.

One circumstance to take into account is that in solar collectors, either FPSC or PVT, the flow that typically occurs is of the forced laminar type, given the low velocity and diameter of the tubes through which the fluid circulates. This produces a temperature field in the fluid section that is far from uniform, as shown by Seco-Nicolás et al. [37]. This field depends on the thermofluidic properties of the fluid and the flow conditions and is related to the concept of characteristic length [38], which marks the length of pipe required for the thermal process to be considered complete and, therefore, the length of pipe required for an efficient use of the pipe, which has undoubted consequences for the design of equipment.

Few works have been devoted to date to study the heat transfer that takes place between the fluid and the tubes of flat plate solar collectors. These studies are limited to conventional thermal collectors and mainly water as heat transfer fluid [37,39], although other collectors and fluids such as thermal oils or ionic liquids [40] have also been studied, reaching the conclusion that the characteristic length of the process is rarely reached in these collectors. The present work addresses the case of a commercial PVT collector, a relatively little studied type of equipment, working with three different fluids: water, ionic liquid [Emim]Ac and a nanofluid based on the previous one by means of experimentation and numerical simulation in order to study the behavior and optimization of these collectors. The results and methodology developed in this work are applicable to other solar thermal collectors. To the authors' knowledge, no similar work has been published to date.

The characteristic process length in tubes subjected to laminar forced convection in asymmetric conditions can be obtained from the evaluation of the thermal field inside the pipe through the free access platform HEATT[®] (HEATT (<https://www.um.es>)) [41,42]. Given that commercial solar collectors are currently designed assuming that the working fluid is water or another fluid with properties of the same numerical order [12], the use of fluids with thermofluidic properties that may be very different requires a specific evaluation of their thermal field and characteristic length.

From ionanofluids (INFs) produced by the addition of graphene nanoparticles (GNP) to 1-ethyl-3-methylimidazolium acetate [Emim]Ac ionic liquids (ILs) characterized by measuring their physicochemical and thermophysical properties [9], the objectives of this work have been the following:

- Test the base ionic liquid and the INF produced as the heat carrier fluid in a commercial solar thermal-photovoltaic hybrid (PVT) collector to compare its performance with that of water and determine the suitability of current PVT collectors for the use of INFs;
- Study by numerical simulation by means of the HEATT application the thermal field inside the PVT collector tubes in order to optimize the tube length and the operating conditions of the collector based on the concept of characteristic length.

The work has been organized: showing after the Introduction, the Materials and the Methods used (Section 2), distinguishing between the heat transfer fluids, the experimental equipment and the computational resources. Due to limitations in the length of the work and because they have been the subject of previous publications [9,41,43], the previous contents are not detailed in the present work. Section 3 presents the results obtained, both in experimentation and in numerical simulation, followed by the discussion of the results (Section 4) and ending with the Conclusions (Section 5), as well as the References and other usual sections in scientific articles.

2. Materials and Methods

2.1. Materials

Water, 1-ethyl-3-methyl-3-methyl-3-methylimidazolium acetate ($\geq 95\%$ purity) or [Emim]Ac, supplied by IoLiTec (Heilbronn, Germany), and ionanofluid (INF) consisting of a 1% mass suspension of graphene nanoparticles in the above ionic liquid, hereafter referred to as Gr-INF, were used as working fluids. To prepare the ionanofluid, physical methods such as agitation and sonication mainly, as well as chemical methods such as covalent or non-covalent functionalization, have been used [44]. Figure 1 schematizes the ionanofluid production process.

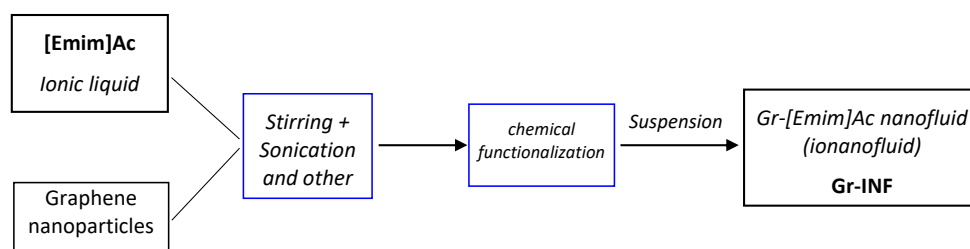


Figure 1. Ionanofluid production process diagram.

The main physicochemical properties measured for the characterization of INF are thermal and electrical conductivities, viscosity, density, specific heat capacity, among other things. The INF produced showed high stability [9]. Table 1 shows the average value of the properties in the temperature range used in this work. For more details, see [9]. Values of IL [Emim]Ac have been obtained from Ionic Liquids Database—ILThermo (<https://www.nist.gov>).

Table 1. Thermophysical properties of water, [Emim]Ac and Gr-INF wt 1% at average temperatures of the fluid (see the table in Section 3.1).

	Water	[Emim]Ac	Gr-INF 1%
Average temperature	41.6	44	44.3
Density, ρ (kg m^{-3})	991.63	1093.18	1096.72
Specific heat, c_p ($\text{J kg}^{-1} \text{K}^{-1}$)	4178.24	1909.96	2050.21
Thermal conductivity, k ($\text{W m}^{-1} \text{K}^{-1}$)	0.635	0.2041	0.2405
Dynamic viscosity, μ (Pa s)	6.38×10^{-4}	0.0083	0.0075

2.2. Solar Collector Tests

Experimental tests were carried out at the Solar Laboratory of the University of Murcia (Spain). The laboratory is equipped with different types of commercial solar collectors, as well as experimental ones, including a hybrid solar thermal-photovoltaic (PVT) collector of the Endef brand (Hybrid solar panel—Endef), in addition to appropriate measuring instrumentation. Figure 2 shows a current image of the plant, showing conventional solar thermal collectors (left), a PVT hybrid collector (in the center, inside the circle) and vacuum tubes (right). The Endef collector is of the riser header configuration [12] or parallel-riser type, in which the inlet (bottom) and outlet (top) of the collector are connected by a set of parallel tubes (risers) through which the heat transfer fluid flows [45].

Figure 3 shows details of the PVT collector installation and instrumentation. Table 2 shows the main dimensions of the PVT collector. The measuring equipment includes the inlet and outlet temperatures of the heat transfer fluid, the flow rate, the solar radiation, as well as the temperature at various points of the absorber plate of the solar collector, so that its actual temperature can be known. The measuring instrumentation is periodically checked and calibrated, and the tests were carried out following the basic indications of the current solar collector testing standards [46].

Table 2. Dimensional characteristics of Endef PVT collector.

Collector length (m)	1.59
Collector width (m)	0.998
Number of risers	9
External tube diameter of the risers, D_e (m)	0.008
Riser tube thickness, e (m)	0.0004
Riser tube length, L (m)	1.52



Figure 2. Solar collectors at the Solar Laboratory of the UMU. Conventional solar thermal collectors (left), PVT hybrid collector (centre) and vacuum tubes (right).

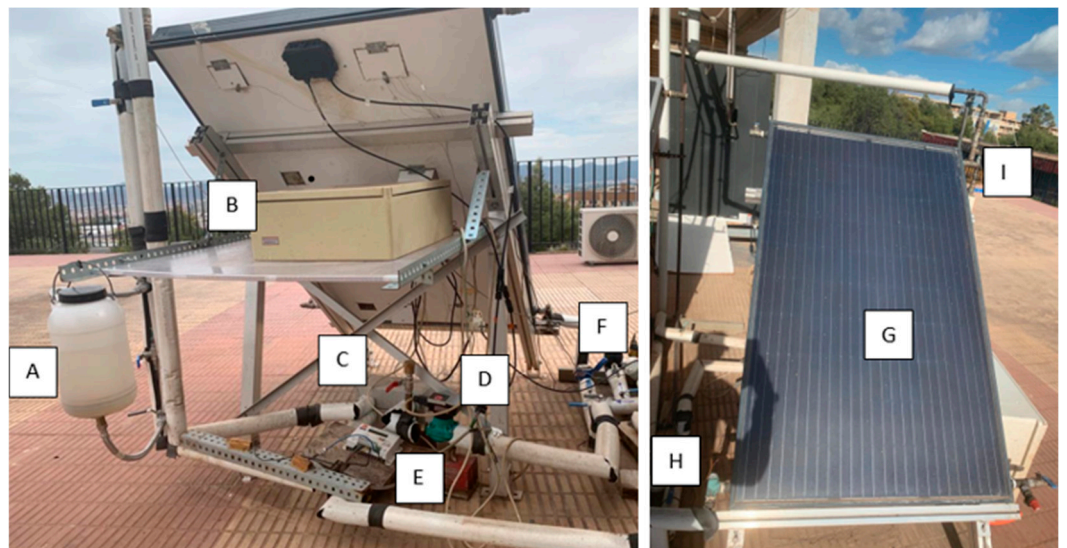


Figure 3. Experimental set of solar PVT panel. (A) Tank, (B) Data logger, (C) Heat exchanger, (D) Pump, (E) Photovoltaic regulator, (F) Flowmeter, (G) Solar panel, (H) Inlet temperature probe and (I) Outlet temperature probe.

The useful heat produced in the solar collector, Q_{col} (W), is accounted by Equation (1), being \dot{m} (kg s^{-1}), the mass flow rate, c_p ($\text{J kg}^{-1} \text{K}^{-1}$), the specific heat of the fluid, and ΔT the temperature jump of the carrier fluid in the collector [10,47].

$$Q_{col} = \dot{m} \cdot c_p (T_{out} - T_{in}) = \dot{m} \cdot c_p \cdot \Delta T, \quad (1)$$

The electrical energy produced, P_{el} , is simply the product of the voltage V (V) and the intensity I (A) generated in the collector, Equation (2) [48].

$$P_{el} = I \cdot V, \quad (2)$$

The thermal efficiency of the collector and the temperature rise of the fluid were analysed in order to show the performance of the PVT collector. The thermal efficiency, denoted as η_{th} , is determined using the stationary efficiency method outlined in the EN 12975-2:2006

standard [47], as well as in the earlier literature [10,25,27,48], Equation (3), with G being the solar irradiance (W m^{-2}).

$$\eta_{th} = \dot{m} \cdot c_p (T_{out} - T_{in}) / S_{col} G \quad (3)$$

The overall collector efficiency can be calculated using Equation (4) [48]:

$$\eta_{ov} = (Q_{col} + P_{el}) / S_{col} G \quad (4)$$

2.3. Numerical Simulation: The HEATT[®] Platform

The numerical simulations have been carried out by means of the HEATT[®] platform [43]. This platform can solve the thermal temperature distribution of homogeneous fluids flowing inside round tubes in a forced laminar regime [41], that usually occurs in solar collectors. The platform is free and easy to use (HEATT (um.es)). It is currently in version 1.0, and a more advanced version is under development.

The HEATT platform is based on the resolution by means of the Network Simulation Method (NSM) of the so-called conjugate-extended Graetz problem subjected to radially asymmetric boundary conditions which makes a 3D model of necessary conditions [49]. The NSM is a numerical simulation method based on the network theory developed by Peusner [50], Horno, González-Fernández [51], Alhama [52] among other researchers, which performs a spatial discretization by finite differences, from which an equivalent electrical circuit is made and solved by means of a circuit solving program. The NSM has been successfully used in the resolution of numerous problems in the field of heat transfer as well as in others (fluid mechanics, strength of materials, membranes, corrosion, geology, etc.).

Essentially, the behavior of a fully developed flow of a Newtonian fluid under forced-laminar convection conditions circulating inside a circular duct in T_{in} is studied under steady state conditions. At a certain point (in this case when the fluid enters the solar collector), the upper part of the external surface of the tube is subjected to the temperature T_{ext} (Figure 4), the lower part of the tube surface being thermally insulated. Consequently, the fluid begins to heat up, ideally, if the tube is long enough, until it reaches the external surface T_{ext} .

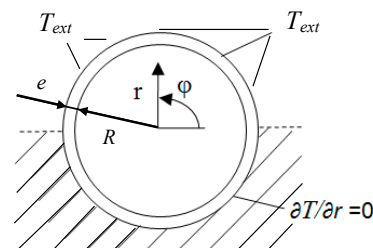


Figure 4. HEATT physical model. Cross section of the tube showing the cylindrical coordinates of the problem and the boundary conditions: upper half of its surface at T_{ext} temperature and lower half thermally insulated.

The model considers heat transfer by conduction through the tube and the fluid itself, both in radial and axial directions. On the other hand, laminar flow avoids mixing of the different fluid layers, while buoyancy is not relevant as there is no natural convection [53]. The conditions required to consider forced laminar flow were established by Suryanarayana [54] and are summarized in compliance with the dimensionless values in Table 3, where ρ is the density, v the fluid velocity, μ the dynamic viscosity, g the gravity acceleration, β the thermal expansion coefficient and ΔT the temperature gradient in the tube surface.

Table 3. Dimensionless numbers for laminar forced convection flow.

Dimensionless Number	Equation	Condition
Reynolds Nr, Re	$Re = \frac{\rho v D}{\mu}$	$1 \times 10^2 < Re < 2 \times 10^3$
Prandtl Nr., $Pr \times D/L$	$Pr \frac{D}{L} = \frac{v D}{\alpha L} = \frac{\mu}{L} \frac{v \cdot \rho \cdot c_p}{k}$	$0.01 < Pr \times D/L < 1$
Rayleigh Nr, Ra	$Ra = Gr \cdot Pr \frac{D}{L} = g \beta \Delta T \frac{D^3}{\nu^2} \frac{v D}{\alpha L} = g \beta \frac{D^4}{\nu} \frac{\Delta T}{L} \frac{\rho \cdot c_p}{k}$	$< 1 \times 10^3$

This process is very similar to that occurring in solar collectors. Flat plate solar thermal collectors are characterized by asymmetric thermal excitation due, on the one hand, to the unidirectional solar irradiation itself and, on the other hand, to the fact that their lower half is thermally insulated to reduce heat losses. For further details on the physical and numerical model, including boundary conditions, see [37,38,41].

Applications of the programme include solar thermal collectors, where their results have been verified [37], and other equipment where the forced laminar flow conditions [54] and the boundary conditions of the problem are satisfied. Although the boundary condition of a solar collector is more similar to that of a constant external heat flow over the surface of the tube, the results of the temperature evolution with the boundary condition used by HEATT (constant external temperature) have been validated in [37] to predict the radially asymmetric temperature field inside the tubes of solar collectors, and under these conditions it is used in the present work.

2.4. Characteristic Length

The so-called characteristic length, L^* , is a hidden quantity, which means that it cannot be measured with standard meters, with different meanings depending on the process. To the one considered in this work, the characteristic length reveals the length needed for the potential heat transfer process to be completed [38,55–57], i.e., when the entire fluid reaches, or at least approaches, the external temperature. In this case, it has been measured as the length needed for the center of the fluid to reach 90% of the external surface temperature.

It is assumed that the characteristic length is an important design criterion: if the tube length is lower than L^* , the thermal potential of the device is not profited. Conversely, if the tube length is greater than L^* , this excess is thermally useless. Figure 5 shows the assessment of the characteristic length in a particular case.

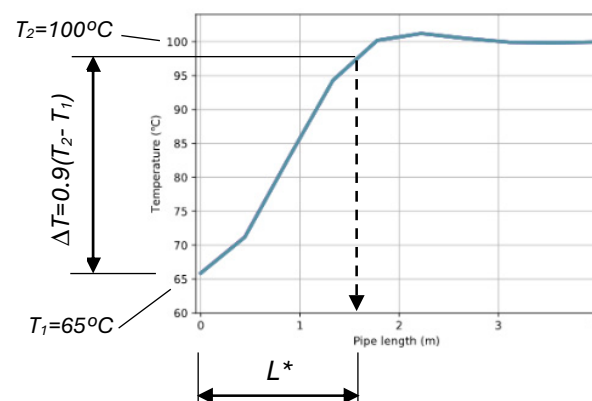


Figure 5. Characteristic length (L^*) assessment in a particular case, where T_1 is the fluid inlet temperature and T_2 the external tube temperature.

3. Results

3.1. Experimental Fluid Temperatures

Although the study of the performance of the hybrid collector is not the main purpose of this work, Table 4 shows representative experimental results for the three fluids flowing

through the PVT collector obtained in three test campaigns carried out for the organizational needs of the laboratory in different seasons. For this reason, the flow rates, irradiances and inlet temperatures, T_{in} , are of the same order but not exactly the same, having been maintained within the range recommended by the standards. Thus, the volumetric flow rates inside the collector, V_{col} , are around $1.2\text{--}2\text{ L s}^{-1}/100\text{ m}^2$ of collectors [58]. The data were obtained in the four central hours of the day, and the irradiances are above 700 Wm^{-2} . These differences in test conditions do not prevent their results from being considered comparable for the purposes of this work. In this sense, the different outlet temperatures, T_{out} , and temperature jump, ΔT_{col} , have their origin more in the characteristics of the fluids than in the test conditions.

Table 4. Experimental results in PVT collector of water, [Emim]Ac ionic liquid (IL) and graphene ionanofluid (Gr-INF).

	\dot{m} (kg s^{-1})	v (m s^{-1})	G (Wm^{-2})	T_{in} ($^{\circ}\text{C}$)	T_{out} ($^{\circ}\text{C}$)	ΔT_{col} (K)	T_{pl} ($^{\circ}\text{C}$)	Q_{col} (W)	P_{el} (W)	η_{th} (%)	η_{ov} (%)
Water	0.0380	0.086	955.7	38.9	44.3	5.4	50.0	862.8	80.0	58.2	63.6
EmimAc	0.0287	0.059	900.0	41.7	46.2	4.5	55.0	250.3	72.9	17.9	23.2
Gr-INF	0.0334	0.068	845.8	38.6	50.3	11.7	67.5	790.9	74.7	60.3	66.0

As can be seen in Table 1, the specific heat of water is more than twice that of ionic liquid (IL) and ionanofluid (Gr-INF), resulting in higher temperature jumps, ΔT_{col} , in Gr-INF with respect to water despite a lower irradiance, G , as can be observed in Table 4; T_{pl} is the plate temperature measured at the top of the absorber plate, which in this work will be considered constant and equal to the outside temperature, T_{ext} , of the problem boundary condition. On the other hand, the useful heat, Q_{col} , and thermal and overall efficiencies, η_{th} and η_{ov} , respectively, show different rates, resulting in Gr-INF obtaining the highest temperature jump and efficiency of the three fluids. Comparing the performance of the PVT collector using water and INF, it is noted that the thermal jump with the latter is more than double that with water and with a better overall energy efficiency (66.0% vs. 63.6%), although the electrical production with INF is somewhat lower than in the case of using water (74.7 W vs. 80 W). Also very striking is the poor thermal performance when using the ionic liquid, which contrasts sharply with that offered by the same substance when forming the ionanofluid with graphene particles.

In the case of electric power, there is not such a wide variation depending on the fluid and its operating conditions. Electricity production, P_{el} , is higher in the case of water, probably due to the lower average temperature of the heat transfer fluid, although the differences are not very pronounced since the temperatures and irradiances are in similar ranges. The best overall performance is obtained when using the Gr-INF.

3.2. HEATT Simulations

The external asymmetry of thermal conditions that occurs in solar thermal devices results in asymmetric temperature fields in the fluid, despite the small diameter of the tube. This is because, as mentioned above, laminar forced convection typically occurs in these devices due to low fluid velocities ($v < 0.1\text{ m s}^{-1}$), as can be seen in Table 4. In addition, the other conditions for laminar forced convection established by Surianarayana [54] are met. Consequently, the HEATT platform can be used to study the temperature field inside the tubes.

Figure 6 shows the simulation results of [Emim]Ac under the conditions of Table 4. The image shows the fluid temperatures along the cross section at different distances ($L/10$ to L , where L is the length of the riser pipe) from the pipe inlet. As can be seen, the fluid temperature is far from homogeneous along the cross section, due to laminar flow and the absence of buoyancy. In the vicinity of the tube inlet ($L/10$), almost all the fluid is at the inlet temperature, which practically does not vary at the end of the tube. Consequently, it can be said that the potential heat transfer process, which would have taken place if all the fluid had ended up at the temperature outside the tube, has not taken place in the tube or,

in other words, that the characteristic length has not been reached for which a longer tube would have been necessary.

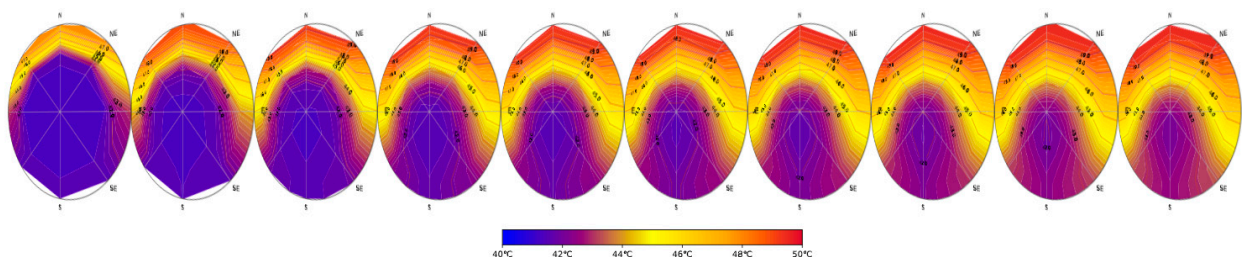


Figure 6. [Emim]Ac steady-state temperature maps of the tube cross sections at different lengths ($L/10$ to L) from the tube inlet. HEATT screenshot. The evolution of the fluid temperature along the tube can be seen with the color code.

Figure 7 shows the results of the simulations of the three fluids of Table 4 inside the PVT collector. Column a shows the evolution of the fluid temperature along the tube for $r = 9/10 R_i$, with R_i being the inner radius of the tube, and different azimuthal angles, named with the acronym of the geographical orientation, i.e., N (north) is the highest point of the fluid, and its plane is the vertical top ($\varphi = 90^\circ$); NE (north-east) corresponds to $\varphi = 45^\circ$; E (east) is the horizontal plane ($\varphi = 0^\circ$); SE (south-east) corresponds to $\varphi = -45^\circ$; and finally, S (south) marks the lower vertical plane and the coldest points of the fluid ($\varphi = 90^\circ$). Remember that the tube is subjected to a temperature higher than that of the fluid at the inlet in its upper half, while it is thermally insulated in its lower half (Figure 4), being symmetrical with respect to the N-S axis. For the simulations, the actual inlet temperature of the fluids in Table 4 has been taken, and the external temperature of the tube, T_{ext} , has been taken as a constant temperature higher than the fluid outlet temperature in each case, being 50.0°C , 55.0°C and 67.5°C for water, IL and INF, respectively, according to measurements carried out on the collector absorber plate (Table 4).

As can be seen in Figure 7, the behavior pattern is quite similar in the three cases. As expected, in the N and NE planes, the fluid temperature at $9/10 R_i$ is very close to that of the outer surface of the tube T_{ext} , while in the S plane, and to a lesser extent in SE, in the vicinity of the thermally isolated zone, the temperature increases slowly without even approaching the outer temperature, leaving the temperature of the S-SE sectors well below the rest of the fluid. As mentioned above, this indicates that in the PVT collector we are far from reaching the characteristic length of the process. Since we are considering a collector of non-modifiable dimensions, the solution to reach the characteristic length would be to reduce the velocity of the fluid so that it would have time to reach this hidden magnitude when passing through the collector.

Column b of Figure 7, on the other hand, shows the thermal field or map of the fluid in the last cross section of the tube, the one located at distance L from the fluid inlet, which coincides with the last one in the screenshot analogous to that of Figure 6. Again, the different temperatures along the fluid section are appreciated, due to the laminar flow characteristics that make fluid mixing difficult. These are higher in the azimuthal planes N and NE and lower in the vicinity of the S plane, where even the point of minimum temperature is somewhat distant from the tube wall: the heat coming from the upper half of the tube is transmitted to the lower half by conduction and from there to the fluid by convection, needing some distance to reach the center of the tube. This circumstance is particularly striking in the case of the ionic liquid [Emim]Ac, due to the lower thermal conductivity of this fluid.

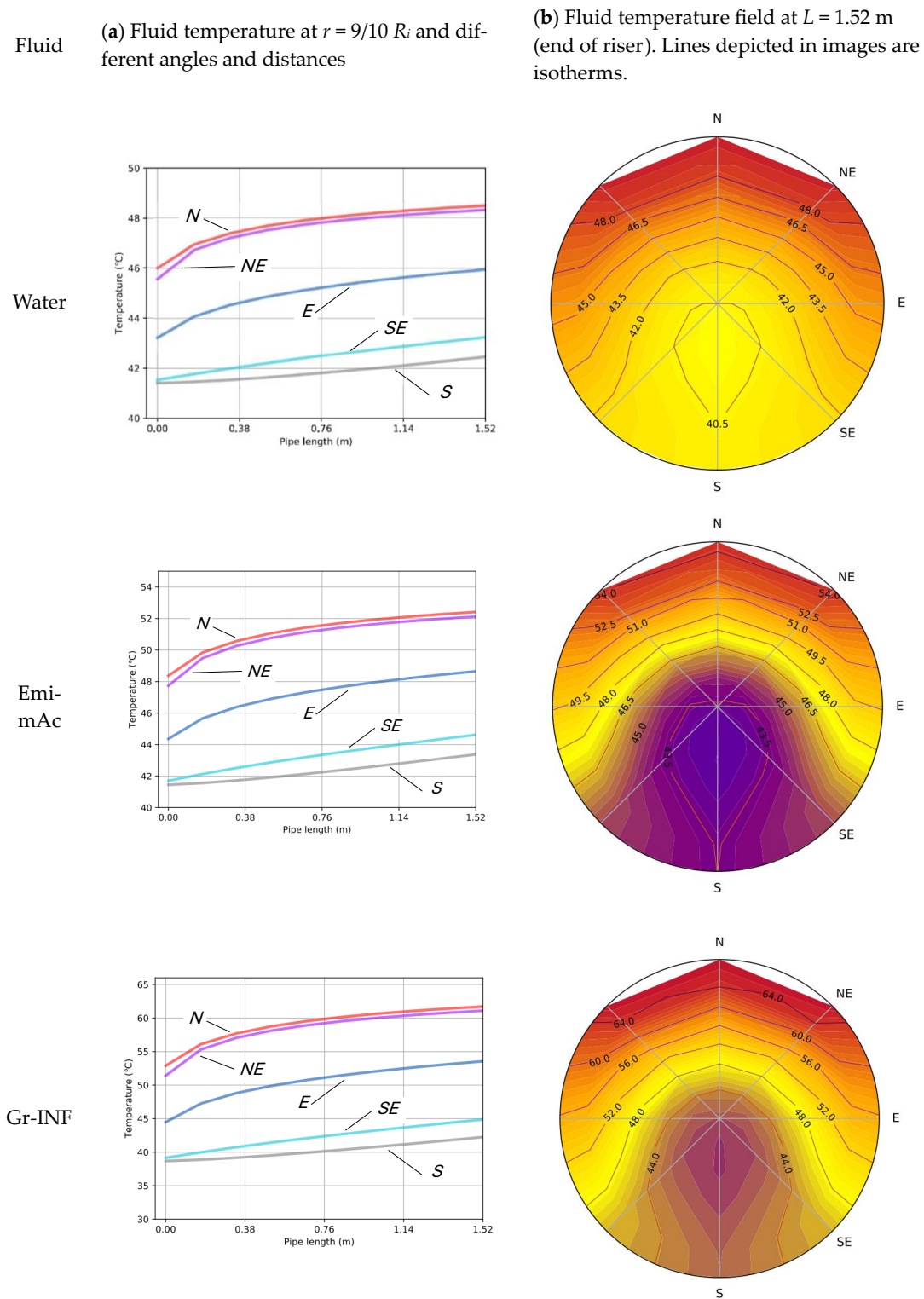


Figure 7. Simulation results of three fluids within PVT collector.

Figure 8 shows the simulations of the INF at three different velocities, the one that follows the flow criterion typically established for solar thermal collectors ($v = 0.068 \text{ m s}^{-1}$) and two slower velocities, $v = 0.023 \text{ m s}^{-1}$ and 0.0068 m s^{-1} . The criterion commonly used for the determination of the characteristic length is that it can be considered reached when the bulk fluid temperature reaches 90% of the thermal gradient jump between the inlet temperature and that of the external condition [57]. In this case ($T_{in} = 38.6 \text{ }^\circ\text{C}$ and

$T_{ext} = 67.5 \text{ }^\circ\text{C}$), this value is $64.6 \text{ }^\circ\text{C}$. The fluid bulk temperature, T_{bulk} , has been assessed as in Equation (5) [53]:

$$T_{bulk} = \frac{\sum S_i \cdot v_i \cdot T_i}{S_i \cdot v_i} \tag{5}$$

where S_i , v_i and T_i are the surface, velocity and temperature of the different section sectors, having obtained these values from dimensions, fluid conditions and the simulation data. Table 5 shows the bulk temperature values for the INF simulations at different flow velocities.

Fluid velocity v (m s^{-1})

(a) Fluid temperature at $r = 9/10 R_i$ and different angles and distances. The coloration of the curves corresponds to the same azimuthal planes as in Figure 7

(b) Fluid temperature field at $L = 1.52 \text{ m}$ (end of riser). Lines depicted in images are isotherms.

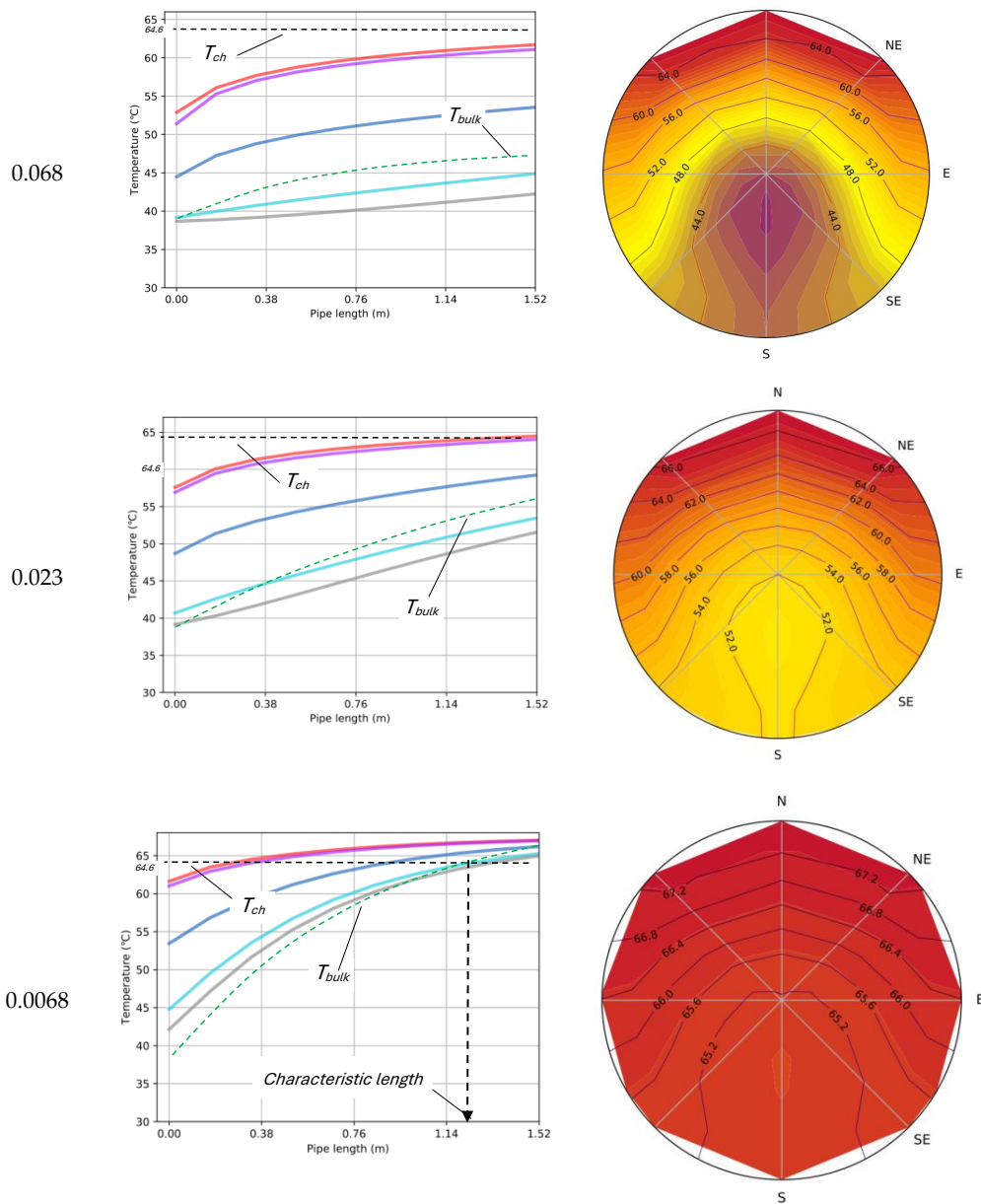


Figure 8. Numerical simulations and determination of the characteristic length for Gr-INF at different fluid velocities.

Table 5. Bulk temperature at the end of the riser ($^{\circ}\text{C}$) for the INF simulations at different flow velocities.

Flow velocity (m s^{-1})	0.068	0.023	0.0068
Bulk temperature ($^{\circ}\text{C}$)	46.7	55.6	66.0

As can be seen in Figure 8, only in the case of $v = 0.0062 \text{ m s}^{-1}$, the characteristic length, L^* , is below that of the collector risers, L ($L = 1.2 \text{ m}$ vs. 1.52 m), and consequently, it can be said that thermal transmission is carried out to the maximum extent possible.

4. Discussion

As Figure 7 shows, fluids working inside commercial PVT solar collectors at the current operating fluid velocity values do not reach the characteristic process length. Only when the fluid velocity is strongly reduced does the characteristic length shorten and lays beyond the collector length, as it shows Figure 7 for the case of Gr-INF. In this case ($v = 0.00682 \text{ m s}^{-1}$), the output temperature is maximum ($66 \text{ }^{\circ}\text{C}$), much higher than in the case of the common flow rate criterium ($v = 0.0682 \text{ m s}^{-1}$), where it only attained $46.7 \text{ }^{\circ}\text{C}$. This is because very slow fluid velocities allow the maximum external temperatures to be reached for the entire fluid.

Table 5 contains the fluid outlet temperatures, heat generated and thermal efficiency of the PVT collector working with Gr-INF at different flow rates and fluid velocities. The data for case 1 corresponds to experimental results (Table 4), while those for cases 2 and 3 are obtained from HEATT results. Consistent with Figure 6 and due to reaching the characteristic length, the temperatures of case 3 are the highest, practically reaching those of the outer surface of the tube, involving an increase of 234%. Compared to the experimental result using water (see Table 4), the temperature increase in case 3 would have been more than five times ($27.4 \text{ }^{\circ}\text{C}$ vs. $5.4 \text{ }^{\circ}\text{C}$). As can be seen, for a given equipment, the variation of the fluid velocity is the easiest means for the variation of the characteristic length of a process.

The collector studied is too short to realize the maximum possible heat transfer, which is partly due to the fact that in a PVT collector both electrical and thermal output are important, and it is known that, in general, high solar cell temperatures penalize electrical output, as the experimental data show (Table 4).

The fluid outlet temperature is an important performance of the collector depending on the application (higher temperatures of a heat carrier fluid have a higher value). In the case of the PVT collector where the heat carrier has a cooling function, in general, increasing the collector temperature is not interesting as it penalizes electricity production, but in other solar applications it can be. The HEATT application is not able to predict the electrical production of the solar collector.

Moreover, as can be seen in Table 6, there is another important consequence of reducing the speed of the fluid, and that is that the useful heat, Q_{col} , produced in the solar collector and the collector thermal efficiency, η_{th} , also decreases significantly (more than four times). In this sense, for the collector under study, if what is of interest is high energy production, the optimal fluid speed would be that which marks the flow recommended by the regulations (case 1).

Table 6. Simulation results for different fluid velocities of Gr-INF in PVT collector on the basis of 845.8 W m^{-2} of solar irradiance.

Case	Mass Flow Rate (kg s^{-1})	v (m s^{-1})	T_{in} ($^{\circ}\text{C}$)	T_{out} ($^{\circ}\text{C}$)	ΔT_{col} (K)	Q_{col} (W)	η_{th} (%)
1	0.0334	0.0682	38.6	50.3	11.7	779.2	59.4
2	0.0113	0.0230	38.6	57.7	19.1	442.5	33.8
3	0.0033	0.0068	38.6	66.0	27.4	188.2	14.4

5. Conclusions

Experimental tests and numerical simulations of three liquids, including water, ionic liquid and graphene ionanofluid of the former ionic liquid, functioning as heat carriers in a commercial PVT solar collector have been performed.

Experimental results show that the best overall performance is obtained when Gr-INF is used, while the poorest results are obtained using the ionic liquid as the thermal carrier. The performance of the PVT collector using INF is even superior to that using water, showing a thermal jump more than double that of water and with a better overall energy efficiency (66.0% vs. 63.6%). Electricity generation is not greatly affected by the fluid used, although when using INF, it is somewhat lower than with water (74.7 W vs. 80 W).

The 3D analysis performed using the HEATT[®] open computing platform reveals that the characteristic length, where the entire heat transfer process occurs, is usually not reached in the parallel-riser PVT collectors used in this research due to the thermal and flow conditions of these devices. In the case of parallel-riser collectors, slower fluid velocities, which allow reaching the characteristic length of the process, are recommended if high outlet temperatures of the fluid are the target of the application, reaching temperature jumps of more than twice of those obtained when using the recommended fluid velocity, but be aware that low fluid velocities strongly penalize thermal and overall energy production. This means that slow fluid velocities are recommended only if high outlet temperatures are desired but bearing in mind that this strongly penalizes thermal energy production.

Longer pipes (i.e., coil type collectors) can improve both performances in PVT solar collectors depending on the application, always taking into account the electrical output of the device. The results and methodology developed in this work are applicable to solar thermal collectors other than PVT collectors.

Ionanofluids may in the medium term become an alternative to water in applications at relatively high temperatures, near or above 100 °C, where water may vaporize or where there are corrosion problems. The ionic liquid tested in the present work, [Emim]Ac, has shown poor results in the solar collector. However, the addition of graphene particles has produced an ionanofluid with performance comparable to that of water, which confirms the validity of this technique for obtaining heat transfer fluids that improve the results of the base fluid. At present, ionic liquids are expensive, but this is expected to decrease in the medium term as their applications increase.

Author Contributions: Conceptualization, M.A.; methodology, M.A. and G.V.; software, M.A., M.S.-N. and J.-P.L.-A.; validation, M.A., M.S.-N. and I.M.; formal analysis, M.A. and J.-P.L.-A.; investigation, M.A. and I.M.; resources, M.A.; data curation, M.A.; writing—original draft preparation, M.A.; writing—review and editing, G.V., M.S.-N. and J.-P.L.-A.; supervision, G.V.; project administration, I.M.; funding acquisition, G.V., M.A., M.S.-N., J.-P.L.-A. and I.M. All authors have read and agreed to the published version of the manuscript.

Funding: This research was partially supported by grants ref. TED2021-130389B-C21, funded by the MCIN/AEI/10.13039/501100011033 project and “NextGenerationEU”/PRTR”; PID2020-113081RB-I00, funded by MCIN/AEI/10.13039/501100011033; and part of 22129-PI-22, funded by the research support program of the Seneca Foundation of Science and Technology of Murcia, Spain. I. Moulefera acknowledges support from Spanish Ministry of Universities under “Margarita Salas program”, financed by the Next Generation EU. The HEATT[®] platform was created through the Proof of Concept project, where the software for calculating the flow in pipes for engineering and architecture was launched as part of the Seneca Foundation of Science and Technology of Murcia, Spain.

Data Availability Statement: All data used in this work are available on request. The HEATT[®] platform, where the numerical simulations were performed, is freely available at HEATT (um.es), and the data necessary to carry out the simulation can be found in the tables of the work. Experimental data supporting the present work can be provided upon request. The simulations performed on the HEATT platform, from which the plots and images in Figures 6–8 have been obtained, can be reproduced at <https://heatt.inf.um.es/en/>.

Conflicts of Interest: The authors declare no conflicts of interest. The funders had no role in the design of the study; in the collection, analyses, or interpretation of data; in the writing of the manuscript; or in the decision to publish the results.

References

1. Council of the European Union and the European Council. European Green Deal. Fit for 55. Available online: <https://www.consilium.europa.eu/en/policies/green-deal/fit-for-55-the-eu-plan-for-a-green-transition/> (accessed on 26 September 2024).
2. Bogdanov, D.; Gulagi, A.; Fasihi, M.; Breyer, C. Full energy sector transition towards 100% renewable energy supply: Integrating power, heat, transport and industry sectors including desalination. *Appl. Energy* **2021**, *283*, 116273. [[CrossRef](#)]
3. Gul, E.; Baldinelli, G.; Bartocci, P.; Shamim, T.; Domenighini, P.; Cotana, F.; Wang, J.; Fantozzi, F.; Bianchi, F. Transition toward net zero emissions—Integration and optimization of renewable energy sources: Solar, hydro, and biomass with the local grid station in central Italy. *Renew. Energy* **2023**, *207*, 672–686. [[CrossRef](#)]
4. Wehbi, H. Powering the Future: An Integrated Framework for Clean Renewable Energy Transition. *Sustainability* **2024**, *16*, 5594. [[CrossRef](#)]
5. Xu, D.; Gu, X.; Dai, Y. Concentrating solar assisted biomass-to-fuel conversion through gasification: A review. *Front. Energy Res.* **2023**, *10*, 1029477. [[CrossRef](#)]
6. Kadam, S.; Dhole, K.; Kumar, A.; Gupta, N.; Mishra, S. Impact of International Solar Alliance on World. *Int. J. Adv. Res. Sci. Commun. Technol.* **2023**, *3*, 261–266. [[CrossRef](#)]
7. Loutzenhiser, P.G.; Muroyama, A.P. A review of the state-of-the-art in solar-driven gasification processes with carbonaceous materials. *Sol. Energy* **2017**, *156*, 93–100. [[CrossRef](#)]
8. Tan, B.; Ke, X.; Tang, D.; Yin, S. Improved perturb and observation method based on support vector regression. *Energies* **2019**, *12*, 1151. [[CrossRef](#)]
9. Moulefera, I.; Pastor, A.R.; Fuster, M.G.; Delgado-Marín, J.J.; Montalbán, M.G.; Rodríguez-Pastor, I.; López-Pérez, A.; Martín-Gullon, I.; Ramallo-González, A.P.; Alarcón, M.; et al. Novel application for graphene oxide-based ionanofluids in flat plate solar thermal collectors. *Sci. Rep.* **2024**, *14*, 17610. [[CrossRef](#)]
10. Duffie, J.A.; Beckman, W.A. *Solar Engineering of Thermal Processes*, 4th ed.; Wiley and Sons: Hoboken, NJ, USA, 2013. [[CrossRef](#)]
11. IEA. Renewables 2022. Available online: <https://www.iea.org/reports/renewables-2022> (accessed on 26 September 2024).
12. Kalogirou, S.A. *Solar Energy Engineering: Processes and Systems*; Elsevier: Amsterdam, The Netherlands, 2023.
13. Ramos, A.; Guarracino, I.; Mellor, A.; Alonso-Álvarez, D.; Childs, P.; Ekins-Daukes, N.J.; Markides, C.N. *Solar-Thermal and Hybrid Photovoltaic-Thermal Systems for Renewable Heating*. Grantham Institute, Briefing Paper No 22; Imperial College: London, UK, 2017. [[CrossRef](#)]
14. Lee, J.; Shin, J. The Economic Value of New Sustainable Products: The Case of Photovoltaic Thermal (PVT) Hybrid Solar Collectors. *Energies* **2023**, *16*, 5473. [[CrossRef](#)]
15. Emmanuel, B.; Yuan, Y.; Maxime, B.; Gaudence, N.; Zhou, J. A review on the influence of the components on the performance of PVT modules. *Sol. Energy* **2021**, *226*, 365–388. [[CrossRef](#)]
16. Khelifa, A.; Touafek, K.; Ben Moussa, H.; Tabet, I.; El Hocine, H.B.C.; Haloui, H. Analysis of a Hybrid Solar Collector Photovoltaic Thermal (PVT). *Energy Procedia* **2015**, *74*, 835–843. [[CrossRef](#)]
17. Dubey, S.; Tiwari, G.N. Analysis of PV/T flat plate water collectors connected in series. *Sol. Energy* **2009**, *83*, 1485–1498. [[CrossRef](#)]
18. Ahmed, M.T.; Rashel, M.R.; Abdullah-Al-Wadud, M.; Hoque, T.T.; Janeiro, F.M.; Tlemcani, M. Mathematical Modeling, Parameters Effect, and Sensitivity Analysis of a Hybrid PVT System. *Energies* **2024**, *17*, 2887. [[CrossRef](#)]
19. Wang, Z.; Hou, G.; Taherian, H.; Song, Y. Numerical Investigation of Innovative Photovoltaic–Thermal (PVT) Collector Designs for Electrical and Thermal Enhancement. *Energies* **2024**, *17*, 2429. [[CrossRef](#)]
20. Margoum, S.; Hajji, B.; Aneli, S.; Tina, G.M.; Gagliano, A. Optimizing Nanofluid Hybrid Solar Collectors through Artificial Intelligence Models. *Energies* **2024**, *17*, 2307. [[CrossRef](#)]
21. Nagarajan, P.K.; Subramani, J.; Suyambazhahan, S.; Sathyamurthy, R. Nanofluids for solar collector applications: A review. *Energy Procedia* **2014**, *61*, 2416–2434. [[CrossRef](#)]
22. Jha, P.; Das, B.; Gupta, R.; Mondol, J.D.; Ehyaei, M.A. Review of recent research on photovoltaic thermal solar collectors. *Sol. Energy* **2023**, *257*, 164–195. [[CrossRef](#)]
23. Said, Z.; Saidur, R.; Rahim, N.A. Energy and exergy analysis of a flat plate solar collector using different sizes of aluminium oxide based nanofluid. *J. Clean. Prod.* **2016**, *133*, 518–530. [[CrossRef](#)]
24. Ganvir, R.; Walke, P.; Kriplani, V. Heat transfer characteristics in nanofluid—A review. *Renew. Sustain. Energy Rev.* **2017**, *75*, 451–460. [[CrossRef](#)]
25. Zayed, M.E.; Zhao, J.; Du, Y.; Kabeel, A.E.; Shalaby, S.M. Factors affecting the thermal performance of the flat plate solar collector using nanofluids: A review. *Sol. Energy* **2019**, *182*, 382–396. [[CrossRef](#)]
26. Wang, W.; Wu, Z.; Li, B.; Sundén, B. A review on molten-salt-based and ionic-liquid-based nanofluids for medium-to-high temperature heat transfer. *J. Therm. Anal. Calorim.* **2019**, *136*, 1037–1051. [[CrossRef](#)]
27. Said, Z.; Hachicha, A.A.; Aberoumand, S.; Yousef, B.A.A.; Sayed, E.T.; Bellos, E. Recent advances on nanofluids for low to medium temperature solar collectors: Energy, exergy, economic analysis and environmental impact. *Prog. Energy Combust. Sci.* **2021**, *84*, 100898. [[CrossRef](#)]

28. Abdelrazik, A.S.; Tan, K.H.; Aslfattahi, N.; Arifutzzaman, A.; Saidur, R.; Al-Sulaiman, F.A. Optical, stability and energy performance of water-based MXene nanofluids in hybrid PV/thermal solar systems. *Sol. Energy* **2020**, *204*, 32–47. [[CrossRef](#)]
29. Aslfattahi, N.; Samyalingam, L.; Abdelrazik, A.S.; Arifutzzaman, A.; Saidur, R. MXene based new class of silicone oil nanofluids for the performance improvement of concentrated photovoltaic thermal collector. *Sol. Energy Mater. Sol. Cells* **2020**, *211*, 110526. [[CrossRef](#)]
30. Liu, J.; Wang, F.; Zhang, L.; Fang, X.; Zhang, Z. Thermodynamic properties and thermal stability of ionic liquid-based nanofluids containing graphene as advanced heat transfer fluids for medium-to-high-temperature applications. *Renew. Energy* **2014**, *63*, 519–523. [[CrossRef](#)]
31. de Castro, C.A.N.; Lourenço, M.J.V.; Ribeiro, A.P.C.; Langa, E.; Vieira, S.I.C.; Goodrich, P.; Hardacre, C. Thermal Properties of Ionic Liquids and Ionanofluids of Imidazolium and Pyrrolidinium Liquids. *J. Chem. Eng. Data* **2010**, *55*, 653–661. [[CrossRef](#)]
32. Shaik, N.B.; Inayat, M.; Benjapolakul, W.; Bakthavatchalam, B.; Barewar, S.D.; Asdornwised, W.; Chaitusaney, S. Artificial neural network modeling and optimization of thermophysical behavior of MXene Ionanofluids for hybrid solar photovoltaic and thermal systems. *Therm. Sci. Eng. Prog.* **2022**, *33*, 101391. [[CrossRef](#)]
33. Józwiak, B.; Dzido, G.; Zorębski, E.; Kolanowska, A.; Jędrysiak, R.; Dziadosz, J.; Libera, M.; Boncel, S.; Dzida, M. Remarkable Thermal Conductivity Enhancement in Carbon-Based Ionanofluids: Effect of Nanoparticle Morphology. *ACS Appl. Mater. Interfaces* **2020**, *12*, 38113–38123. [[CrossRef](#)]
34. Zhang, F.-F.; Zheng, F.-F.; Wu, X.-H.; Yin, Y.-L.; Chen, G. Variations of thermophysical properties and heat transfer performance of nanoparticle-enhanced ionic liquids. *R. Soc. Open Sci.* **2019**, *6*, 182040. [[CrossRef](#)]
35. Hasečić, A.; Almutairi, J.H.; Bikić, S.; Džaferović, E. Numerical analysis of heat transfer performances of ionic liquid and ionanofluids with temperature-dependent thermophysical Properties. *Energies* **2021**, *14*, 8420. [[CrossRef](#)]
36. Das, L.; Habib, K.; Saidur, R.; Aslfattahi, N.; Yahya, S.M.; Rubbi, F. Improved Thermophysical Properties and Energy Efficiency of Aqueous Ionic Liquid/MXene Nanofluid in a Hybrid PV/T Solar System. *Nanomaterials* **2020**, *10*, 1372. [[CrossRef](#)] [[PubMed](#)]
37. Seco-Nicolás, M.; Alarcón, M.; Luna-Abad, J.P. 3D numerical simulation of laminar forced-convection flow subjected to asymmetric thermal conditions. An application to solar thermal collectors. *Sol. Energy* **2021**, *220*, 230–245. [[CrossRef](#)]
38. Seco-Nicolás, M.; Alarcón, M.; Alhama, F. Thermal behavior of fluid within pipes based on discriminated dimensional analysis. An improved approach to universal curves. *Appl. Therm. Eng.* **2018**, *131*, 54–69. [[CrossRef](#)]
39. Maré, T.; Galanis, N.; Voicu, I.; Miriel, J. Experimental analysis of mixed convection in inclined tubes. *Appl. Therm. Eng.* **2006**, *26*, 1677–1683. [[CrossRef](#)]
40. Alarcon, M.G.; Seco-Nicolas, M.; Luna-Abad, J.P.; Ramallo-Gonzalez, A.P. 3D analysis of forced laminar flows in pipes subjected to asymmetric external conditions. In Proceedings of the International Heat Transfer Conference 17, Cape Town, South Africa, 14–18 August 2023. [[CrossRef](#)]
41. Seco-Nicolás, M.; García, M.A.; González, A.P.R.; Luna-Abad, J.P. HEATT©. A free software for thermal design of liquid flows inside pipes. *Results Eng.* **2023**, *17*, 100983. [[CrossRef](#)]
42. Alarcón, M.; Nicolás, M.S.; Luna-Abad, J.P.; Ramallo-González, A.P. Forced Laminar Flow in Pipes Subjected to Asymmetric External Conditions: The HEATT© Platform for Online Simulations. In *Pipeline Engineering—Design, Failure, and Management*; Rushd, S., Ismail, M., Adane, K.F., Eds.; IntechOpen: London, UK, 2022; p. 20. [[CrossRef](#)]
43. Alarcón, M.; Seco-Nicolás, M.; Luna-Abad, J.P.; Ramallo-González, A.P.; Heatt. Online. Available online: <https://heatt.inf.um.es/en/> (accessed on 26 September 2024).
44. Bo, L.; Zhang, X.; Luo, Z.; Saboori, T.; Dehghan, M.; Ghasemizadeh, M.; Karimi-Maleh, H.; Alagumalai, A.; Mahian, O. An overview of the applications of ionic fluids and deep eutectic solvents enhanced by nanoparticles. *J. Therm. Anal. Calorim.* **2022**, *147*, 7589–7601. [[CrossRef](#)]
45. Abora Energy, S.L. SHE: Solar Heat & Electricity. Available online: <https://abora-solar.com/en/she-project/> (accessed on 26 September 2024).
46. ISO 9806:2017; Solar Energy. Solar Thermal Collectors. Test Methods. International Organization for Standardization (ISO): Geneva, Switzerland, 2017.
47. EN 12975-2:2006; Thermal Solar Systems and Components—Solar Collectors—Part 2 Test Methods. AENOR: Madrid, Spain, 2006.
48. Gagliano, A.; Tina, G.M.; Aneli, S.; Nižetić, S. Comparative assessments of the performances of PV/T and conventional solar plants. *J. Clean. Prod.* **2019**, *219*, 304–315. [[CrossRef](#)]
49. Bilir, Ş. Numerical solution of graetz problem with axial conduction. *Numer. Heat Transf. Part A Appl.* **1992**, *21*, 493–500. [[CrossRef](#)]
50. Peusner, L. Network thermostatics. *J. Chem. Phys.* **1985**, *83*, 1276–1291. [[CrossRef](#)]
51. González-Fernández, C.F. Heat Transfer and the Network Simulation Method. In *Network Simulation Method*; Horno, J., Ed.; Research Signpost: Kerala, India, 2002.
52. Alhama, F.; López-Sánchez, J.F.; González-Fernández, C.F. Transient heat conduction in a plate with variable thermal conductivity and non-linear boundary conditions by network simulation method. *Rev. Mex. Fis.* **1999**, *45*, 449–453.
53. Incropera, F.P.; DeWitt, D.P.; Bergman, T.L.; Lavine, A.S. *Fundamentals of Heat and Mass Transfer*; John Wiley & Sons: Hoboken, NJ, USA, 2007; Volume 6. [[CrossRef](#)]
54. Suryanarayana, N.V. Forced Convection—Internal Flows. In *The CRC Handbook of Thermal Engineering*; Kreith, F., Ed.; CRC Press LLC: Boca Raton, FL, USA, 2000; pp. 3-47–3-55.

55. Madrid, C.N.; Alhama, F. Discrimination: A fundamental and necessary extension of classical dimensional analysis theory. *Int. Commun. Heat Mass Transf.* **2006**, *33*, 287–294. [[CrossRef](#)]
56. Cánovas, M.; Alhama, I.; Alhama, F. Mathematical Characterization of Bénard-Type Geothermal Scenarios Using Discriminated Non-dimensionalization of the Governing Equations. *Int. J. Nonlinear Sci. Numer. Simul.* **2015**, *16*, 23–34. [[CrossRef](#)]
57. Madrid, C.N.; Alhama, F. Discriminated dimensional analysis of the energy equation: Application to laminar forced convection along a flat plate. *Int. J. Therm. Sci.* **2005**, *44*, 333–341. [[CrossRef](#)]
58. ASIT. Guía IDAE 022: Guía Técnica de Energía Solar Térmica, V 1.0. Madrid (Spain): Instituto de Diversificación y Ahorro de la Energía (IDAE). Online. 2020. Available online: <https://www.idae.es/publicaciones/guia-tecnica-de-energia-solar-termica> (accessed on 26 September 2024).

Disclaimer/Publisher’s Note: The statements, opinions and data contained in all publications are solely those of the individual author(s) and contributor(s) and not of MDPI and/or the editor(s). MDPI and/or the editor(s) disclaim responsibility for any injury to people or property resulting from any ideas, methods, instructions or products referred to in the content.